Fabric and Effective Stress Distribution in Internally Unstable Soils

Fabric and effective stress distribution in internally unstable soils

Shire, T.[1]; O'Sullivan, C. [2]; Hanley, K.J. [3]; Fannin, R.J. [4]

1: PhD Candidate, Department of Civil and Environmental Engineering, Imperial College, London, SW7 2AZ, United Kingdom

2: Reader in Particulate Soil Mechanics, Department of Civil and Environmental Engineering, Imperial College, London, SW7 2AZ, United Kingdom

3: Research Associate, Department of Civil and Environmental Engineering, Imperial College, London, SW7 2AZ, United Kingdom

4: Professor, Department of Civil Engineering, University of British Columbia, Vancouver, V6T 1Z4, Canada.

This is an author generated postprint of the article:

Shire, T., O'Sullivan, C., Hanley, K. J., & Fannin, R. J. (2014). Fabric and effective stress distribution in internally unstable soils. *Journal of Geotechnical and Geoenvironmental Engineering*, *140*(12).

http://dx.doi.org/10.1061/(ASCE)GT.1943-5606.0001184

Abstract

Internal instability is a form of internal erosion in broadly-graded cohesionless soils in which fine particles can be eroded at lower hydraulic gradients than predicted by classical theory for piping or heave. A key mechanism enabling internal instability is the formation of a stress-transmitting matrix dominated by the coarse particles that leaves the finer particles under lower effective stress. In this study discrete element modeling is used to analyze the fabric and effective stress distribution within idealized gap-graded samples with varying potential for internal stability. The reduction in stress within the finer fraction of the materials is directly quantified from grain-scale data. The particle size distribution, percentage finer fraction and relative density are found to influence the stress distribution. In particular, effective stress transfer within a critical finer fraction between 24% and 35% is shown to be highly sensitive to relative density.

Introduction

Internal instability is a form of internal erosion which occurs in broadly and gap-graded cohesionless and low-plasticity soils (ICOLD 2013), when the coarse fraction of the soil is unable to prevent the erosion of the fine fraction under the action of seepage. Moffat et al. (2011) draw a distinction between two types of internal instability, namely suffusion and suffosion. Where suffusion occurs, the finer particles are eroded through the coarse fraction "without any loss of [the load-carrying] matrix integrity or change in total volume", whereas finer particle migration due to suffosion "yields a reduction in total volume and a consequent potential for collapse of the soil matrix". Cohesionless soils can be subjected to backward erosion, contact erosion or suffusion depending on their position with respect to seepage direction and level of internal stability (ICOLD 2013, Wan and Fell 2004).

Internal instability occurs under the combined influence of three factors: *(i)* material susceptibility, *(ii)* critical stress condition and *(iii)* critical hydraulic load, shown in Venn diagram form in Figure 1 (after Garner and Fannin 2010). This paper focuses on the critical stress condition and the material susceptibility, specifically the distribution of stress between particles of different sizes in a potentially unstable gradation.

Material susceptibility essentially refers to the material fabric and there are two key aspects. Firstly, the fine particles must be small enough to pass through the constrictions in the void network between the coarser particles (a geometric criterion). Secondly, the finer particles must not completely fill the voids between the coarse particles so that they carry a relatively low stress and are transportable under seepage (a stress criterion). Two important finer fraction values were identified by Skempton and Brogan (1994). Firstly, the critical finer fraction (S*) at which the finer particles fill the voids, which was estimated to fall between the narrow limits of finer fractions by mass, F_{fine} = 24% to 29% for dense and loose samples respectively, based on assumed minimum and maximum porosities. Secondly, the finer fraction S_{max} at which the finer particles completely separate the coarse particles from one another, which Skempton and Brogan proposed is given as F_{fine} = 35%. Other aspects of material susceptibility which could contribute towards internal instability include inhomogeneity, low relative density, material segregation (ICOLD 2013) and stress anisotropy (Chang and Zhang 2013).

If the two material susceptibility criteria (geometric and stress) are met, internal instability will initiate if a critical hydraulic gradient is applied to the soil. This critical gradient is lower than would be expected to cause failure by heave, as found experimentally by Skempton and Brogan (1994), Wan and Fell (2004) and Fannin and Moffat (2006) amongst others. Skempton and Brogan (1994) postulated a grain-scale explanation, whereby the majority of the effective stress is carried by a matrix of coarse particles, leaving the loose finer particles under relatively low stress. These less-stressed fine particles reach a zero effective stress state, and become potentially mobile, at lower hydraulic gradients than would be expected from an examination of the average stress.

To quantify this effect, they proposed that a stress-reduction factor, α, can be defined as the proportion of the overburden acting on the loose fraction in the "no flow condition" i.e.:

$$\sigma'_{fine} = \alpha\, \sigma' \qquad 1$$

where: σ'_{fine}: effective stress transferred by the finer fraction; σ': overburden effective stress; α: stress-reduction factor.

Combining the stress-reduction factor with Terzaghi's classic theory for heave at zero effective stress, the critical hydraulic gradient for a cohesionless soil with no surface loading becomes:

$$i_c = \alpha^{lab} \gamma'/\gamma_w \qquad 2$$

where: i_c: critical hydraulic gradient for internal instability; γ': buoyant unit weight; γ_w : unit weight of water. Note that when α = 1, the soil is internally stable and Equation 2 becomes the Terzaghi relationship. Equation 2 implies that α^{lab} is an indirect measurement obtained permeameter tests.

Using a stress-controlled permeameter, Moffat and Fannin (2011) found a linear relationship between effective stress level and critical hydraulic gradient for internally unstable soils. Li and Fannin (2012) subsequently proposed that the stress-reduction factor α is practically constant over a range of stress levels, allowing them to derive a generalized form of Equation 2 that can account for any imposed effective stress. The critical hydraulic gradient at the base of a soil element for upward flow becomes:

$$i_c = \alpha\, (\bar{\sigma}'_{v0} + \gamma'/\gamma_w) \qquad 3$$

where $\bar{\sigma}'_{v0}$ is the normalized vertical effective stress, $\bar{\sigma}'_{v0} = \sigma'_{v0}/\gamma_w\ h$, σ'_{v0} is the applied vertical effective stress at the top of the specimen and *h* is the length over which the hydraulic gradient is measured. The vertical effective stress is divided by h in order to take into account the decrease with h of critical hydraulic gradient observed by Li (2008) and Marot et al. (2012a). Equations 2 and 3 are formulated for upward seepage flow. However, Moffat and Fannin (2011) and Li (2008) show the onset of instability in stress-gradient space appears independent of whether upwards or downwards flow direction was used.

Although the α-concept is based on hypothesized grain-scale behavior, the experimentally determined values on which the concept relies were calculated by comparing the observed critical hydraulic gradient to the theoretical value for heave. It is not experimentally possible to directly measure the stress in the finer soil fraction.

A number of studies indicate that the role of the fine particles varies with finer fraction. For example, based on the results of direct shear tests on gap graded mixtures of glass beads, Vallejo (2001) concluded that at $F_{fine} \leq$ 30% the shear strength was controlled primarily by the coarse particles with the finer fraction sitting loose within the voids, at F_{fine} = 30 - 60% both coarse and finer fractions contribute and at F_{fine} > 60% the finer fraction

alone controlled the strength. Thevanayagam et al. (2002) developed five fabric cases to classify the liquefaction potential of sands with non-plastic silt fines, and these are likely to have a broader application:

(i) finer particles are fully confined within voids between coarse particles and provide no support to the coarse particles;

(ii) finer particles are partially in contact with and provide some support to coarse particles;

(iii) most finer particles are confined within voids but some finer particles separate coarse particles from one another, increasing the fragility of the soil;

(iv) :

1. coarse and fine particles both contribute towards shear strength;

2. coarse particles are fully dispersed within a matrix of finer particles, which control shear strength

Cases (i) to (iii) refer to finer fractions < S*, whereas (iv-1) and (iv-2) refer to finer fractions > S*. Case (i) materials are often referred to by dam engineers as "underfilled" (ICOLD 2013) and if the geometric criterion is met these materials are susceptible to suffusion (i.e. $\alpha \approx 0$). In relation to internal stability, Case (iii) materials can be considered a special form of Case (i) material, in which most finer particles are unstressed and susceptible to suffusion, but the few which are trapped between coarse particles are highly stressed. Case (iv) materials are "overfilled" and internally stable ($\alpha \approx 1$). Case (ii) materials may be susceptible to suffosion if the stress in the fines supporting the coarse particles is low enough for them to be preferentially eroded and the geometric criterion is met.

Discrete element modeling (DEM) is a numerical technique originally proposed by Cundall and Strack (1979) that allows a quantitative grain-scale assessment of the fabric of idealized granular materials. Shire and O'Sullivan (2013) used DEM to analyze the relationship between grain-scale fabric and the empirical criterion for assessing internal stability proposed by Kézdi (1979) for a series of idealized gap-graded soils with varying particle size distribution (PSD) and finer fractions at a single relative density level. The average number of inter-particle contacts per particle fell as instability increased, representing an increase in the proportion of loose, erodible fine particles. Similarly, the number of coarse particles participating in stress transfer fell as instability increased.

The objective of this study is to use DEM to further investigate the aspects of soil fabric which contribute towards internal instability. The DEM dataset used comprises larger samples than those considered by Shire and O'Sullivan (2013) and includes a wider range of finer fractions and relative densities. In particular the distribution of effective stress within a soil is examined by using the inter-particle contact force data provided in the DEM simulations to directly calculate α. The support provided to the soil matrix by the finer fraction is examined using α and the number of contacts each particle has with its neighbors. Following a comparison of the DEM α values with experimental data, the relationships between α and various micro- and macro-scale

parameters are explored through a systematic variation of gap-ratio, finer fraction and relative density. Emphasis is placed on the sensitivity of effective stress transmission through the finer particles to the critical finer fraction values identified by Skempton and Brogan (1994).

PSDs considered

A total of 16 gradations were considered as detailed in Figure 2 and Table 1. The largest particle in each numerical specimen was 10 mm in diameter. Referring to Table 1, the susceptibility to instability is quantified according to two commonly used empirical criteria: *(i)* the $(D'_{15}/d'_{85})_{max}$ ratio first proposed by Kézdi (1979), where D′ represents the coarse fraction and d′ the finer fraction; *(ii)* the $(H/F)_{min}$ ratio proposed by Kenney and Lau (1985), where F is the % by mass of the soil smaller than a diameter D, and H is the % passing between D and 4D.

There is one linear gradation, termed "Dam Filter", with a PSD matching that of a granular filter collected from a dam under construction in southern Europe. Being linear, Dam Filter does not have distinct coarse and fine fractions but has been given a nominal F_{fine} = 50% to indicate that it can be considered "overfilled". The remaining 15 gradations are gap-graded. Two of the gap-gradations are similar to those considered in prior experimental research: "FR7" has approximately the same PSD as a physical specimen of spherical glass beads that was tested at the University of British Columbia (Li 2008) with a finer fraction of 30% and a gap ratio (D'_0 /d'_{100}) of 5.7. Skempton A is similar to the gradations "A" tested by Skempton and Brogan (1994) and "HF01" tested by Li (2008), both of which consisted of real sands and gravels. The finer fraction is 13% and the gap ratio is approximately 4. Both gradations are considered internally unstable by both the Kézdi and the Kenney and Lau criteria. However, as shown in Figure 2(a) while the PSDs are similar, the coarse fraction of the experimental samples is more widely graded than the DEM sample. This was necessary in order to limit the number of particles required and allow the simulations to run within a reasonable time.

The remaining 13 gap-gradations belong to one of three series of PSDs with varying finer fractions and gap ratios but very uniform coarse and fine fractions. Each of these is named either "Gap Narrow XX", "Gap Med XX" or "Gap Wide XX" where XX is a number representing the finer fraction by % mass. The Gap Narrow gradations have a gap ratio of 3 and are internally stable according to the Kézdi and Kenney and Lau criteria, the Gap Med gradations have a gap ratio of 4 and are borderline unstable according to the Kézdi method and unstable according to the Kenney and Lau criterion. The Gap Wide gradations have a gap ratio of 7.5 and are unstable according to both the Kézdi and the Kenney and Lau criteria.

The coarser and finer fractions for each gradation in the "Gap" series are very uniform, with Cu = 1.2. This was necessary in order to reduce the total number of DEM particles required, and the computational resources required for the simulations. However, for these PSDs the Kenney and Lau criterion provides a very sharp distinction in stability, with gradations with gap ratio = 3 being classified as highly stable, and those with gap ratio = 4 being highly unstable. For the same gradations the Kézdi criterion varies almost linearly with gap ratio.

Additionally, Li and Fannin (2008) found that the Kézdi criterion was more successful than the Kenney and Lau criterion at predicting internal instability in gap-graded soils. Therefore the Kézdi criterion is used as an empirical measure of internal stability in the remainder of the discussion here. The idealized gap-gradings used here allowed easy identification of the coarse and fine fractions. In a broadly-graded sample, the point at which the PSD should be split into coarse and fine fractions is not clear. The work to date on this issue is summarized in ICOLD (2013).

DEM Simulations

The DEM simulations were carried out on cubic samples using a modified version of the open-source DEM code Granular LAMMPS (Plimpton 1995). Periodic boundary conditions were used to create a sample which is effectively of infinite size and is free from the boundary effects associated with rigid boundaries, allowing particle numbers to be kept to a reasonable level. A Hertz-Mindlin contact model was used and the simulation input parameters were Poisson's ratio $\nu = 0.3$, shear modulus $G = 27.0$ GPa and particle density $\rho = 2670$ kg/m^3, which are approximately equal to experimentally derived values for spherical glass beads used by Barreto (2008). Particles are initially placed in random, non-touching positions within the periodic cell using an in-house placement code, creating a fully homogeneous, high porosity sample, which then undergoes periodic compression.

The periodic compression method for sample generation proposed by Cundall (1988) was used here. The periodic boundaries and the particles contained within move as if part of a continuum subjected to a uniform strain field. In addition to the particle movement due to the imposed strain field, during compression, particles also moved due to the resultant force of all contact forces. A stress-controlled servo-control algorithm imposed a strain rate that reduced as the initial target isotropic stress level of $p' = (\sigma'_1 + \sigma'_2 + \sigma'_3) / 3 = 50$ kPa was approached, where σ'_1 , σ'_2 , σ'_3 are the three principal stresses. This modeling and simulation approach has been used by Thornton (2000) amongst others. In order to achieve a range of final void ratios, different coefficients of inter-particle friction were used during the compression stage, i.e. $\mu = 0.0$, $\mu = 0.1$ and $\mu = 0.3$, which are termed "dense", "medium" and "loose" respectively. This yielded a more systematic variation in packing density than has hitherto been achieved or considered in experimental studies. To allow a consistent comparison of the results, the friction was changed to $\mu = 0.3$ for all samples when $p' = 50$ kPa. Each simulation had a minimum of 500 coarse particles; a parametric study in which the number of particles was varied showed this was sufficient to achieve a representative element volume (REV), meaning there was no statistically significant change in the results with an increase in the number of particles within the periodic cell. Further details are given in Shire (2014).

A large number of particles (up to 304,205) and a very wide range of particle sizes were used, meaning that the computational cost of the simulations was very high. In order to run such demanding simulations, this work made use of the UK's national high-performance computing service, HECToR, and the Curie HPC facility, which was accessed through the European PRACE program. Even with these state of the art facilities, the larger

simulations required a run time of several weeks to complete. The size of the simulations necessitated the use of spherical particles. Although this is an idealization of real sands, and particle shape is known to affect the filtration properties of sands (Marot et al., 2012b), prior experimental research has also used spherical glass beads to remove the influence of shape and the justification for empirical design rules such as Kézdi (1979) and Kenney and Lau (1985) also assume spherical particles. The samples were homogeneous and isotropic, and gravity was neglected. Neglecting gravity is necessary where periodic boundaries are used and it results in some samples having coordination numbers, Z, less than one (Z = the average number of inter-particle contacts per particle in a sample). This allows easy identification of those particles which are participating in effective stress transfer. Were gravity to be enabled, and a rigid base boundary added in place of periodic boundaries, the minimum coordination number would be 1 as the unconnected particles would fall to rest on other particles. However, those particles would still not participate in stress transmission. This approach means that factors known to affect internal stability such as stress-induced anisotropy and soil inhomogeneity cannot be considered.

Simulations were terminated when the mean normal stress reached the target level and coordination number remained constant for 20,000 simulation cycles. The mechanical coordination number, Z_{mech}, is the number of contacts per particle considering only particles with two or more contacts, i.e. those particles that are likely to transmit stress. Four samples generated with $\mu = 0.3$ reached a stable $p' = 50$ kPa with Z^{mech} remaining constant and < 4, for over 1,000,000 DEM cycles. In these simulations fine particles become trapped between two larger particles, creating a meta-stable fabric similar to Case (iii) proposed by Thevanayagam et al. (2002). To ensure that the samples were as stable as possible an additional simulation termination rule was adopted where, considering particles with two contacts only, less than 0.5% of contacts were "sliding" i.e., $F_t = \mu F_n$, where F_t is tangential contact force and F_n is normal contact force.

An important aspect of internal stability is the size of the inter-void constrictions between the stress transmitting matrix. While it is possible to determine constriction sizes within DEM samples (e.g. Shire et al. 2013), here the focus is on the role which finer particles play in the stress transmitting matrix . The stress acting on the fines will control the initiation of erosion; the constriction sizes are relevant for controlling subsequent particle transport and should be considered in future DEM analyses looking at progression of soil erosion.

Calculation of stress-reduction factor

Equations 1 to 3 were developed to consider the heterogeneity of the stress transfer within an internally unstable soil. In a DEM model the smallest volume over which stress can be quantified is a single particle, although in reality the stress distribution within a particle is highly heterogeneous (Russell et al. 2009). Potyondy and Cundall (2004) give an expression for the average stress tensor within a particle, $\bar{\sigma}_{ij}^{p}$, loaded solely by $N_{c,p}$ point contact forces:

$$\bar{\sigma}_{ij}^{p} = \frac{1}{V^{p}} \sum_{c=1}^{N_{c,p}} f_{j}^{c} \left(x_{i}^{c} - x_{i}^{p} \right) \quad 4$$

where: V^{p} and x_{i}^{p}: particle volume and centroidal position; f_{j}^{c}: contact force transmitted at contact position x_{i}^{c}. The average stress tensor for a sample consisting of N_{p} particles and their surrounding void space is:

$$\sigma'_{ij} = \frac{1}{V} \sum_{p=1}^{N_{p}} \left(\bar{\sigma}_{ij}^{p} V^{p} \right) \quad 5$$

where: V is the total sample volume (solid + void). As an isotropic stress state has been used for all DEM simulations presented here, the α-factor is defined in terms of the mean normal stress p'.

$$p'_{fine} = \alpha^{DEM} p' \quad 6$$

Following Equation 5, the mean normal stress for the sample is calculated using:

$$p' = \frac{1}{V} \sum_{p=1}^{N_{p}} (p^{p} V^{p}) \quad 7$$

where: p^{p}: particle mean normal stress. The mean normal stress for the finer fraction is:

$$p'_{fine} = \frac{(1-n)}{\sum_{N_{p,fine}} V^{p}} \sum_{p=1}^{N_{p,fine}} (p^{p} V^{p}) \quad 8$$

where: n: sample porosity; $N_{p,fine}$: number of particles belonging to the finer fraction. Note that Equation 2, which defines α^{lab}, fundamentally differs from Equations 6 – 8, and α^{DEM} can be > 1. Consequently one cannot expect α^{lab} to equal α^{DEM}.

Relationship between α and $(D'_{15}/d'_{85})_{max}$

The void ratio (e), coordination number (Z), and stress-reduction factor (α^{DEM}) for DEM simulations at p'=50 kPa are presented in Table 2. Figure 3 shows the relationship between $(D'_{15}/d'_{85})_{max}$ and α^{DEM} for all the numerical simulations carried out, α^{lab} for Skempton A, FR7 and a database of experimental results compiled by Li (2008) with additional data from Wan and Fell (2004). The best fit line to the experimental data found by Li (2008) is also included. Each DEM data point is colored by the relative density of the sample. Note that for a selected number of simulations the mean normal stress was increased to p' = 200 kPa in 25 kPa increments. The α-factor was found to be practically constant over this stress range (Shire, 2013).

It is important to firstly compare the direct DEM measurements (α^{DEM}) with the indirect experimentally-derived values (α^{lab}). The stress-reduction α-factor calculated from the DEM simulations for Skempton A ranged from $\alpha^{DEM} = 0.04$ for the dense sample to $\alpha^{DEM} = 0.15$ for the loose sample. Experimentally, Skempton and Brogan (1994) obtained $\alpha^{lab} = 0.18$ using a 139mm diameter permeameter while Li (2008) reported $\alpha^{lab} = 0.13$ using a 279mm diameter permeameter. Both experimental studies used a specimen preparation technique in which the material was placed moist in the permeameter and was not densified prior to testing. It is therefore not unreasonable to compare these physical specimens to the loose DEM specimen, and so the agreement can be considered good. On the other hand, the DEM calculated stress-reduction factor for specimen FR7 is highly sensitive to relative density. $\alpha^{DEM} = 0.19$, 0.70 and 1.17 for the loose, medium and dense states respectively. A value of $\alpha^{DEM} > 1$ signifies that the calculated stress is slightly higher in the finer particles than in the coarser particles. These high values are a consequence of the stress definition adopted. While this conflicts with the upper limit of $\alpha=1$ implied by Equation 2, α^{DEM} can reasonably be taken as an index of stability and so the calculated values are presented in all tables and figures here. Experimentally, Li (2008) found $\alpha^{lab} = 0.07$ as the best-fit to a number of experiments using 102 mm and 279 mm diameter permeameters. FR7 was also tested using a preparation technique which would result in a loose specimen. The loose DEM state also shows the finer particles to be carrying just a fraction of the overall stress ($\alpha^{DEM,loose} = 0.19$ and $\alpha^{lab} = 0.07$), therefore the agreement between numerical and experimental results is reasonable for the loose case, although there is a very wide range of scatter in the DEM results.

It is not surprising that better agreement between experimental and numerical analyses is found for Skempton A than FR7. Skempton A has a finer fraction of around 13%, far below the critical finer fraction. The finer particles will therefore sit loose and understressed within the voids, regardless of relative density. FR7, with $F_{fine} = 30\%$ sits within the transitional limits of 24% and 35% from under to overfilled. Within these limits a change in relative density causes a dramatic change in fabric as the voids between the coarse particles become just too small to contain the finer particles. This is demonstrated by the large increase in coordination number with density as shown in Table 2 for FR7. This represents the large number of finer particles making contact with one another and with the coarse particles. The micro-structural response of gap-graded soils above, below and within these limits is studied in the following sections.

Referring to finer fraction values in Table 1 and void ratio values in Table 2, within each "Gap" series of PSDs the minimum void ratio was reached at 25% finer fraction for the medium and dense samples, and for the loose samples it was found at 30% finer fraction for Gap Narrow and Gap Med, and at 35% finer fraction for Gap Wide. One would expect to find the critical finer fraction at the minimum void ratio (Skempton and Brogan 1994) and, as the critical finer fraction should also reduce with increasing relative density, it is no surprise that this pattern should be found. However, although void ratio may highlight where the critical finer fraction is for a given gap-grading and within a given grading α increases with decreasing e, when all samples are considered together there is apparently no relationship between e and α.

Considering the entire dataset presented on Figure 3, the general trend for both experimental and numerical data is of decreasing α with $(D'_{15}/d'_{85})_{max}$. However, within these data there is considerable scatter, showing that $(D'_{15}/d'_{85})_{max}$ alone is insufficient to characterize the effective stress distribution. Referring to Figure 3, the available experimental data indicate that samples with $(D'_{15}/d'_{85})_{max} < 5$ are internally stable (e.g. Fannin and Moffat 2006) as the finer particles are too large to be transported through the constrictions between the coarse particles, regardless of finer fraction and how much stress they carry. Samples with $(D'_{15}/d'_{85})_{max} > 7$, which fail the geometric condition, have a tendency to be highly unstable, but can also be internally stable, depending on finer fraction. Where finer particles are loose and under-stressed, they will be able to migrate through the voids – it is therefore the stress in the finer fraction which controls internal stability for these samples. The DEM results, which measure only stress and do not account for whether loose finer particles may be transported through the voids, show a large degree of scatter and a high dependency on relative density. In the following sections the macro and micro-scale variables that can be measured in DEM will be used to examine changes in fabric which can give a scientific framework to this apparent scatter.

Analysis of factors influencing α

The data presented in Figure 3 indicate the absence of a simple relationship between α and $(D'_{15}/d'_{85})_{max}$. Recalling the discussion on finer fraction by Skempton and Brogan (1994), the relationship between F_{fine} and α is presented in Figure 4 with a schematic showing the change in fabric with F_{fine}. The Dam Filter sample has been assigned a nominal $F_{fine} = 50\%$. Three types of behavior can be observed:

(i) $\alpha < 0.4$ at $F_{fine} < 24\%$: underfilled behavior (coarse grain supported fabric). Finer particles carry reduced stress and will be mobile if the geometric condition is met.

(ii) $\alpha > 0.8$ at $F_{fine} > 35\%$: overfilled behavior: Fine and coarse play approximately equal roles in stress transfer. The material should be internally stable.

(iii) transitional behavior for $24\% < F_{fine} < 35\%$: α is highly sensitive to relative density, with $\alpha > 0.75$ typically for dense samples and $\alpha < 0.5$ typical for loose samples. There is a trend of increasing α with F_{fine}.

The transitional zone is bound by the limits identified by Skempton and Brogan (1994) (S^* and S_{max}). As can be seen in Figure 4, within the transitional zone the samples with the largest gap-ratios have lower α-values than those with smaller gap-ratios. For any given sample with $F_{fine} > 24\%$ α generally increases with relative density. For some samples with $F_{fine} < 24\%$ α decreases with increasing relative density. This response is tentatively attributed to the stress transmitting matrix becomes more stable as the relative density increases.

Figure 5(a) and (b) present the variation of α with $(D'_{15}/d'_{85})_{max}$ for the loose and dense states respectively. In each case trend lines are drawn for samples with a specific finer fraction, and the Dam Filter sample is taken as an internally stable benchmark. In the loose state, samples of all finer fractions show a reduction in α as the $(D'_{15}/d'_{85})_{max}$ ratio increases. This comprises a large initial reduction between $(D'_{15}/d'_{85})_{max} \approx 2$ and $(D'_{15}/d'_{85})_{max} \approx 6$, with a less significant reduction thereafter. At high $(D'_{15}/d'_{85})_{max}$ ratios, the finer particles are smaller than the voids between the coarse particles, meaning they can pack efficiently within the voids and sit loose with little interaction with the load-carrying coarse particles, whereas at low $(D'_{15}/d'_{85})_{max}$ ratios the finer particles mismatch with the coarse particle voids and the resulting interaction causes the finer particles to join the stress-transfer mechanism. This is shown schematically in Figure 5(a). The reduction in α with $(D'_{15}/d'_{85})_{max}$ is replicated at the other densities for the samples with $F_{fine} \leq 18\%$. For samples with $F_{fine} \approx 25\%$ the α values increase with density, but a sharp reduction in α is still observed with $(D'_{15}/d'_{85})_{max}$. Samples with $F_{fine} \geq 30\%$ are sensitive to density, and have an internally stable fabric in medium and dense states, with $\alpha \approx 1$.

Micro-scale analysis of α

Figure 6 shows the relationship between the proportion of particles forming the load-carrying matrix, P_{strong}, and α, where the load-carrying matrix is defined by those particles which participate in the "strong force chains", i.e. those carrying at least one above average magnitude contact force. There is a strong relationship between P_{strong} and α, indicating that if even a small number of coarse particles form a stress transmitting matrix, the fines carry reduced stress.

A more detailed look at the role of the finer fraction is possible by considering partial coordination numbers (Minh and Cheng 2013). Figure 7(a) shows the variation of α with fine coordination number, where:

$$Z^{fine} = \frac{\sum_{i=1}^{N_{p,fine}} (C_i^{fine-fine} + C_i^{fine-coarse})}{N_{p,fine}} \quad (9)$$

where Z^{fine}: fine coordination number; $N_{p,fine}$: total number of fine particles; $C_i^{fine-fine}$: number of contacts between fine particle *i* and other fine particles; $C_i^{fine-coarse}$: number of contacts between particle *i* and coarse particles.

A similar result is obtained if α is plotted against the overall coordination number, Z (Shire, 2013). In gap-graded soils fine particles are far more numerous than the coarse, even when their volumetric proportion is much

lower. This means that $Z_{fine} \approx Z$. Here, Z_{fine} is considered to emphasise that it is the role of the finer particles in fabric and stress-transfer which is being considered. In Figure 7(a) three types of fabric can be identified, each of which is similar to a fabric case identified by Thevanayagam et al. (2002), as shown schematically in Figure 7(b). Each fabric case can be related to one of the three types of internal erosion identified by Moffat et al. (2011): suffusion, suffosion and piping. The micro-mechanical boundaries for the cases here are $Z^{fine} = 2$, which represents the minimum value at which finer particles are on average connected to the stress-transfer mechanism, and $\alpha = 0.5$. Case (i) and Case (iii) soils could be susceptible to suffusion (if the geometric criterion is met). They have fabrics in which the finer particles are generally loose. The finer particles may be susceptible to erosion at low hydraulic gradients but as they are unconnected to the stress-transfer matrix their loss would not threaten stability. These fabrics emerge in soils which are underfilled, i.e. the finer particles are insufficient to fill the voids between the coarse particles. Case (ii) may represent soils which are susceptible to suffosion. The finer particles in these materials carry low stress rather than being loose, and they are connected to the stress-transfer matrix so their loss would threaten matrix stability. This is because although effective stress is transferred by highly stressed particles in strong force chains, these strong force chains are prevented from collapsing due to lateral support from weaker forces, as shown by Tordesillas et al. (2009) and illustrated schematically in Figure 7(b). This type of fabric will emerge in soils in which there is a relatively large size ratio between coarse and fine (allowing the finer particles to pack efficiently in the voids) and which have finer fractions around the critical value (F_{fine} = 25-35%). Case (iv) materials have a stress-transfer matrix which is well distributed between coarse and fine. These materials would be internally stable but could be susceptible to other forms of internal erosion (e.g. piping).

The cases can be further illustrated by examining the fabric evolution of sample Gap Med 25, which for the loose, medium and dense states has Case (i), (ii) and (iv) fabrics respectively. Figure 8(a) gives the proportion of coarse-coarse, coarse-fine and fine-fine contacts in the loose, medium and dense samples, and Figure 8(b) gives the proportion of contact types of above average magnitude or "strong" contacts only. Figure 8(a) also includes the α-factor for each sample. The loose sample, with Case (i) fabric is dominated by coarse-coarse and coarse-fine contacts. Only around 10% of all contacts are between two fine particles, and almost all of these are of below average magnitude. The coarse-coarse contacts make up around 2/3 of all above average magnitude contacts, and unsurprisingly they dominate stress-transfer, as illustrated by $\alpha = 0.18$. In the medium sample, which has Case (ii) fabric, most contacts in the sample are between fine particles. Coarse-coarse contacts make up only around 2% of all contacts in the sample, but around 20% of strong contacts. Fine-fine contacts make up 60% of all contacts, but only around 30% of strong contacts. This demonstrates that many finer particles will carry only weak contact forces, and will therefore be understressed. The overall contact fabric of the dense sample is similar to the medium sample. However, fine-fine contacts play a more prominent role in the strong contact fabric indicating that the finer particles play a larger role in stress-transfer. This is also demonstrated by the difference in the stress-reduction factor, with $\alpha = 0.33$ and 0.76 for the medium and dense samples respectively.

Conclusions

This paper presents a micro-scale analysis of an observed macro-scale phenomenon, internal instability. A total of 48 DEM simulations at three relative density levels, covering a wide range of gap-gradations as well as a uniform gradation were carried out. Analyses of the results of these simulations provide theoretical evidence to confirm the hypothesis by Skempton and Brogan (1994), supported experimentally by Moffat and Fannin (2011), that internal instability can occur at lower hydraulic gradients than would be required for failure by heave or piping because finer particles carry less stress than would be expected from looking at the average stress conditions alone. The reduction in stress in the finer fraction is quantified by the α-factor, which is calculated at the micro-scale using DEM variables. Where the simulations could be directly compared to existing experimental data with similar gap-ratios and fines contents, the agreement was reasonable. Although the gradings are not identical, they are believed to be similar enough to warrant comparison. Systematic variation of the PSD and relative density allowed a more thorough consideration of the factors influencing stress heterogeneity (i.e. α) than had hitherto been possible experimentally.

Figure 3 generally supports the experimental finding of Li (2008) that there is a relationship between α and $(D'_{15}/d'_{85})_{max}$. However the analyses presented in Figures 4 and 6 show the significant influence of the percentage finer fraction and relative density on α, which is not captured in the simple $(D'_{15}/d'_{85})_{max}$ index. Taking account of the discussion presented by Skempton and Brogan (1994) that the finer fraction is critical to understanding stress-transfer in gap-graded soils and looking in detail at the DEM simulation data, a conceptual framework summarizing the key factors affecting stress-transfer is proposed. Referring to Figure 9, α depends on both $(D'_{15}/d'_{85})_{max}$ and F_{fine}. It is clear that the sensitivity of α to $(D'_{15}/d'_{85})_{max}$ depends on whether the soil is overfilled, underfilled or transitional. In all cases if $(D'_{15}/d'_{85})_{max}$ is low, the finer particles are of similar size to the voids, and can therefore become part of the stress transfer mechanism, and α approaches 1. As $(D'_{15}/d'_{85})_{max}$ increases, the size of the finer particles relative to the voids decreases and the particles can completely fit within the voids. For these soils, α will depend on the percentage finer fraction, F_{fine}. Skempton and Brogan (1994) proposed that the critical finer fraction below which the finer particles will play a diminished role in stress-transfer was S* = 24-29% depending on relative density, with an upper limit at S_{max} = 35% above which the finer particles would completely separate the coarser particles from one another and the material will be internally stable. Referring to Figure 4, Skempton and Brogan's limits seem to be broadly appropriate, although it should be noted that even at F_{fine} = 35% some of the loose samples continue to transmit reduced stress through the finer fraction.

From the DEM data, if the F_{fine} < 25%, the soil can be considered underfilled and the finer particles will sit loose in the voids. If the finer particles can fit through the constrictions in the void network, there is potential for the suffusion form of internal instability. If F_{fine} > 35%, the soil is overfilled, where the finer particles completely fill the voids and stress transfer is shared between coarse and fine. Overfilled soils can be considered internally stable.

The behavior of transitional soils which fall between Skempton and Brogan's critical upper and lower limits S* and S_{max} is poorly understood and had not previously been studied in detail. For these soils α is determined by the relative density of the material, and an increase in relative density significantly enhances the stress in the finer fraction and therefore internal stability. This finding has a practical relevance as in soils with $F_{fine} \geq 25\%$ which may be susceptible to internal instability, remedial work to increase the in situ relative density should yield an increase in stability. However, soils with $F_{fine} < 25\%$ would not see a significant increase in stability with densification.

Fabric categories identified by Thevanayagam et al. (2002) for the liquefaction potential of sands with non-plastic silts are useful to describe the fabric of internally unstable soils. Three types of fabric which overlap with one or more of the cases proposed by Thevanayagam et al. can be identified at the micro-scale, in particular by examining the number and magnitude of contacts between particles. Each fabric type identified could be susceptible to one of three forms of internal erosion identified by Moffat et al. (2011):

1. Case (i) and (iii) materials, in which the coarse particles dominate stress transfer and the finer particles sit loose within the voids between. These materials are susceptible to suffusion, i.e. the finer particles can be eroded with no loss of matrix integrity.

2. Case (ii) materials, in which the coarse particles dominate stress transfer, but the well-connected but understressed finer particles play a supporting role. These materials are susceptible to suffosion, i.e. the finer particles can be removed by hydraulic gradients less than would be expected to cause heave, but their removal would cause some rearrangement of the load-carrying matrix.

3. Case (iv) materials, in which coarse and fine both form an integral part of the load-carrying matrix. These materials are internally stable could be susceptible to other forms of internal erosion (e.g. piping).

Acknowledgements

Computing resources from Research Councils UK's HECToR HPC (via EPSRC grant EP/I006761/1), the European PRACE Program and the CX1 HPC at Imperial College are gratefully acknowledged. The first author was funded by an EPSRC Doctoral Training Account.

References

Barreto, D. (2008). *Numerical and experimental investigation into the behaviour of granular materials under generalised stress states.* PhD, Imperial College London.

Chang, D. S., & Zhang, L. M. (2013). Critical Hydraulic Gradients of Internal Erosion under Complex Stress States. *Journal of Geotechnical and Geoenvironmental Engineering, 139*(9), 1454-1467.

Cundall, P.A. (1988). Computer simulations of dense sphere assemblies. *Micromechanics of granular materials, 4*, 113-123.

Cundall, P.A., & Strack, O.D.L. (1979). A discrete numerical model for granular assemblies. *Géotechnique, 29*(1), 47-65.

Fannin, R.J, & Moffat, R. (2006). Observations on internal stability of cohesionless soils. *Géotechnique, 56*(7), 497-500.

Garner, S. J. and Fannin R. J. (2010). Understanding internal erosion: a decade of research following a sinkhole event. *International Journal on Hydropower and Dams. 17*(3): 93-98.

ICOLD. (2013). *Bulletin on internal erosion of dams, dikes and their foundations: Volume 1*. Paris: ICOLD.

Kenney, T. C., & Lau, D. (1985). Internal Stability of Granular Filters. *Canadian Geotechnical Journal, 22*(2), 215-225.

Kézdi, Á. (1979) *Soil physics: Selected topics*, Elsevier.

Li, M. (2008). *Seepage induced instability in widely graded soils.* (PhD), University of British Columbia.

Li, M. & Fannin, R.J. (2008) Comparison of two criteria for internal stability of granular soil. *Canadian Geotechnical Journal.* 45 (9).

Li, M. & Fannin, R.J. (2012). A theoretical envelope for internal instability of cohesionless soil. *Géotechnique, 62*(1), 77-80.

Marot, D., Le, V. D., Garnier, J., Thorel, L., & Audrain, P. (2012). Study of scale effect in an internal erosion mechanism: centrifuge model and energy analysis. *European Journal of Environmental and Civil Engineering, 16*(1), 1-19.

Marot, D., Bendahmane, F., & Nguyen, H. H. (2012). Influence of angularity of coarse fraction grains on internal erosion process. *La Houille Blanche*, (6), 47-53.

Minh, N.H., & Cheng, Y.P. (2013). A DEM investigation of the effect of particle-size distribution on one-dimensional compression. *Géotechnique, 63*(1), 44-53.

Moffat, R., & Fannin, R. J. (2011). A hydromechanical relation governing internal stability of cohesionless soil. *Canadian Geotechnical Journal, 48*(3), 413-424.

Moffat, R., Fannin, R. J., & Garner, S. J. (2011). Spatial and temporal progression of internal erosion in cohesionless soil. *Canadian Geotechnical Journal, 48*(3), 399-412.

Plimpton, S. (1995). Fast Parallel Algorithms for Short-Range Molecular-Dynamics. *Journal of Computational Physics, 117*(1), 1-19.

Potyondy, D. O., & Cundall, P. A. (2004). A bonded-particle model for rock. *International Journal of Rock Mechanics and Mining Sciences, 41*(8), 1329-1364.

Russell, A. R., Muir Wood, D., & Kikumoto, M. (2009). Crushing of particles in idealised granular assemblies. *Journal of the Mechanics and Physics of Solids, 57*(8), 1293-1313.

Shire, T. (2014) *Micro-scale modelling of granular filters.* (PhD), Imperial College London.

Shire, T., & O'Sullivan, C. (2013). Micromechanical assessment of an internal stability criterion. *Acta Geotechnica, 8*(1), 81-90.

Shire, T., O'Sullivan, C., Barreto, D., & Gaudray, G. (2013). Quantifying stress-induced anisotropy using inter-void constrictions. *Geotechnique, 63*(1), 85-91.

Skempton, A. W., & Brogan, J. M. (1994). Experiments on Piping in Sandy Gravels. *Géotechnique, 44*(3), 449-460.

Thevanayagam, S, Shenthan, T, Mohan, S, & Liang, J. (2002). Undrained fragility of clean sands, silty sands, and sandy silts. *Journal of geotechnical and geoenvironmental engineering, 128*(10), 849-859.

Thornton, C. (2000). Numerical simulations of deviatoric shear deformation of granular media. *Geotechnique, 50*(1), 43-53.

Tordesillas, A., Zhang, J., & Behringer, R. (2009). Buckling force chains in dense granular assemblies: physical and numerical experiments. *Geomechanics and Geoengineering: An International Journal, 4*(1), 3-16.

Vallejo, L. E. (2001). Interpretation of the limits in shear strength in binary granular mixtures. *Canadian Geotechnical Journal, 38*(5), 1097-1104.

Wan, C. F. & Fell, R. (2004). Experimental investigation of internal instability of soils in embankment dams and their foundations. *UNICIV Report R429*, Univ. of New South Wales.

Sample	**Particles**	**F_{fine} (%)**	**$(D'_{15}/d'_{85})_{max}$**	**$(H/F)_{min}$**
Skempton A	172684	13	11.7(unstable)	0.21 (unstable)
FR7	176082	30	7.0 (unstable)	0.06 (unstable)
Dam Filter	20083	N/A	1.4 (stable)	2.2 (stable)
Gap Med 18	19997	18	4.6 (borderline unstable)	0.13 (unstable)
Gap Med 25	36928	25	4.5 (borderline unstable)	0.13 (unstable)
Gap Med 30	39595	30	4.5 (borderline unstable)	0.09 (unstable)
Gap Med 35	50357	35	4.5 (borderline unstable)	0.13 (unstable)
Gap Med 45	81297	45	4.4 (borderline unstable)	0.57 (unstable)
Gap Narrow 18	8563	18	3.4 (stable)	2.33 (stable)
Gap Narrow 25	13205	25	3.4 (stable)	2.33 (stable)
Gap Narrow 30	16810	30	3.4 (stable)	2.33 (stable)
Gap Narrow 35	19304	35	3.4 (stable)	1.93 (stable)
Gap Wide 18	114287	18	8.6 (unstable)	0.08 (unstable)
Gap Wide 25	187488	25	8.4 (unstable)	0.05 (unstable)
Gap Wide 30	267329	30	8.4 (unstable)	0.13 (unstable)
Gap Wide 35	304205	35	8.4 (unstable)	0.13 (unstable)

Table 1. PSDs used for DEM analysis.

Sample	Relative density	α	e	Z
Skempton A	Loose	0.15	0.370	0.01
	Medium	0.06	0.332	0.01
	Dense	0.04	0.299	0.01
FR7	Loose	0.19	0.278	0.17
	Medium	0.70	0.247	4.90
	Dense	1.17	0.225	5.82
Dam Filter	Loose	0.91	0.463	2.62
	Medium	1.01	0.435	3.82
	Dense	1.09	0.394	5.04
Gap Med 18	Loose	0.17	0.443	0.17
	Medium	0.10	0.381	0.18
	Dense	0.13	0.303	0.24
Gap Med 25	Loose	0.18	0.348	0.15
	Medium	0.33	0.289	3.09
	Dense	0.76	0.262	5.33
Gap Med 30	Loose	0.24	0.320	0.64
	Medium	1.05	0.299	4.41
	Dense	0.99	0.274	5.55
Gap Med 35	Loose	0.34	0.325	3.08
	Medium	0.86	0.317	4.62
	Dense	1.15	0.288	5.63
Gap Med 45	Loose	0.77	0.403	3.74
	Medium	1.05	0.380	4.84
	Dense	1.16	0.336	5.78
Gap Narrow 18	Loose	0.31	0.474	0.47
	Medium	0.28	0.405	0.65
	Dense	0.39	0.337	1.19
Gap Narrow 25	Loose	0.40	0.402	0.62
	Medium	0.56	0.345	2.36
	Dense	0.94	0.317	5.11
Gap Narrow 30	Loose	0.49	0.379	1.21
	Medium	0.80	0.352	3.95
	Dense	1.06	0.323	5.43
Gap Narrow 35	Loose	0.58	0.385	2.29
	Medium	0.88	0.366	4.39
	Dense	1.14	0.333	5.58
Gap Wide 18	Loose	0.09	0.445	0.03
	Medium	0.04	0.385	0.02

	Dense	0.02	0.307	0.03
Gap Wide 25	Loose	0.12	0.325	0.03
	Medium	0.03	0.233	1.66
	Dense	0.22	0.200	5.50
Gap Wide 30	Loose	0.17	0.295	0.04
	Medium	0.80	0.246	4.89
	Dense	1.17	0.224	5.86
Gap Wide 35	Loose	0.23	0.277	3.77
	Medium	0.86	0.266	4.92
	Dense	1.19	0.241	5.87

Table 2. Coordination number, mechanical coordination number, void ratio and stress-reduction factor values for each simulation.

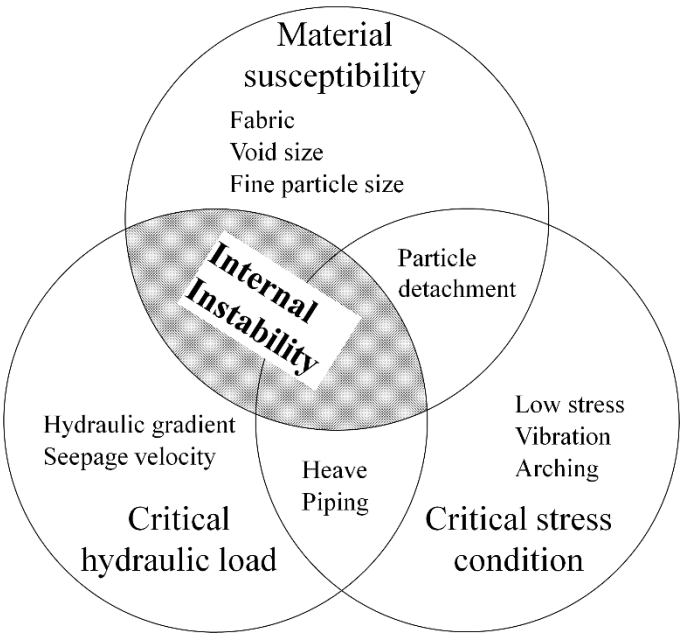

Figure 1. *Venn diagram showing contributory factors to internal instability* (adapted from Garner and Fannin 2010)

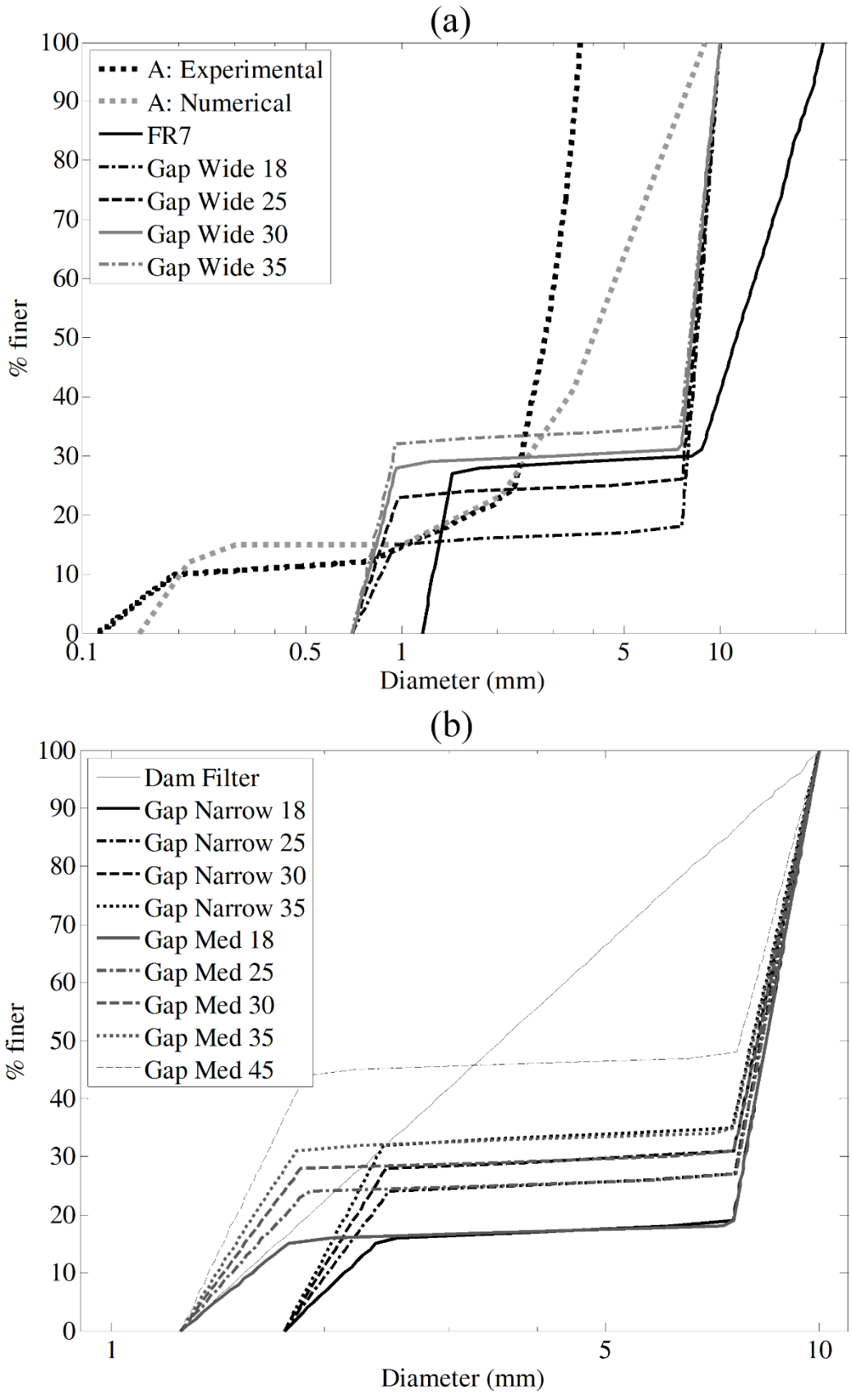

Figure 2. PSDs of samples analyzed: (a) Wider gradations; (b) Narrower gradations.

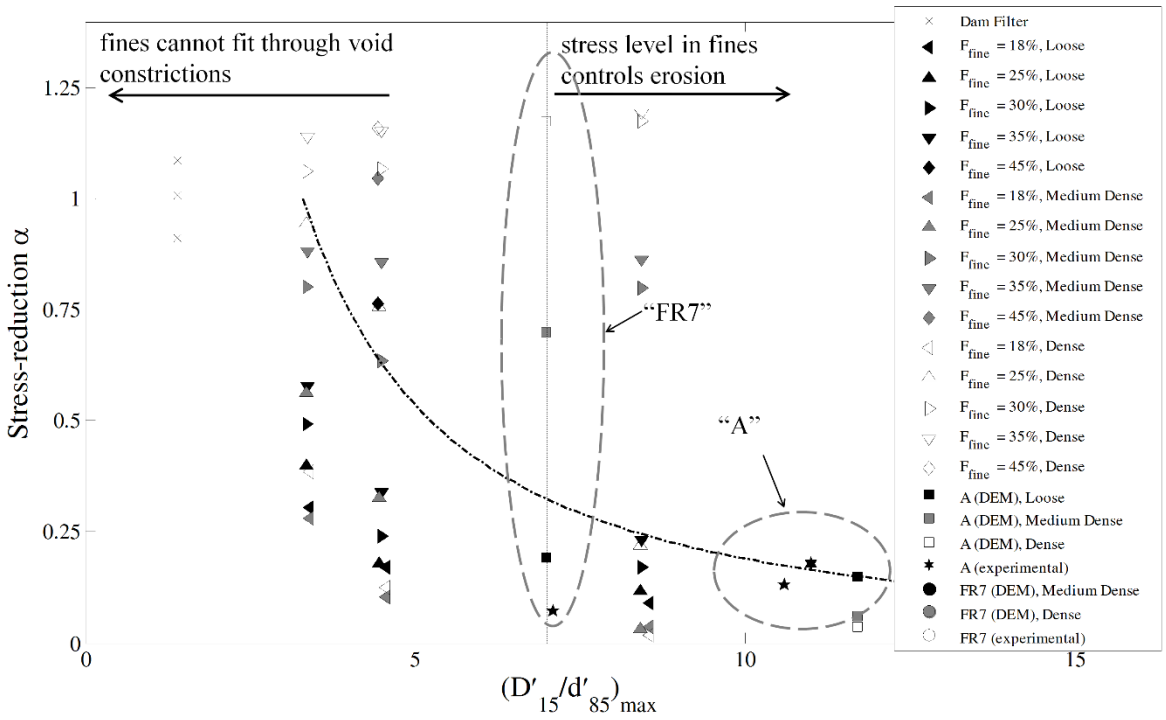

Figure 3. Variation of α with $(D'_{15} / d'_{85})_{max}$ for DEM and experimental data

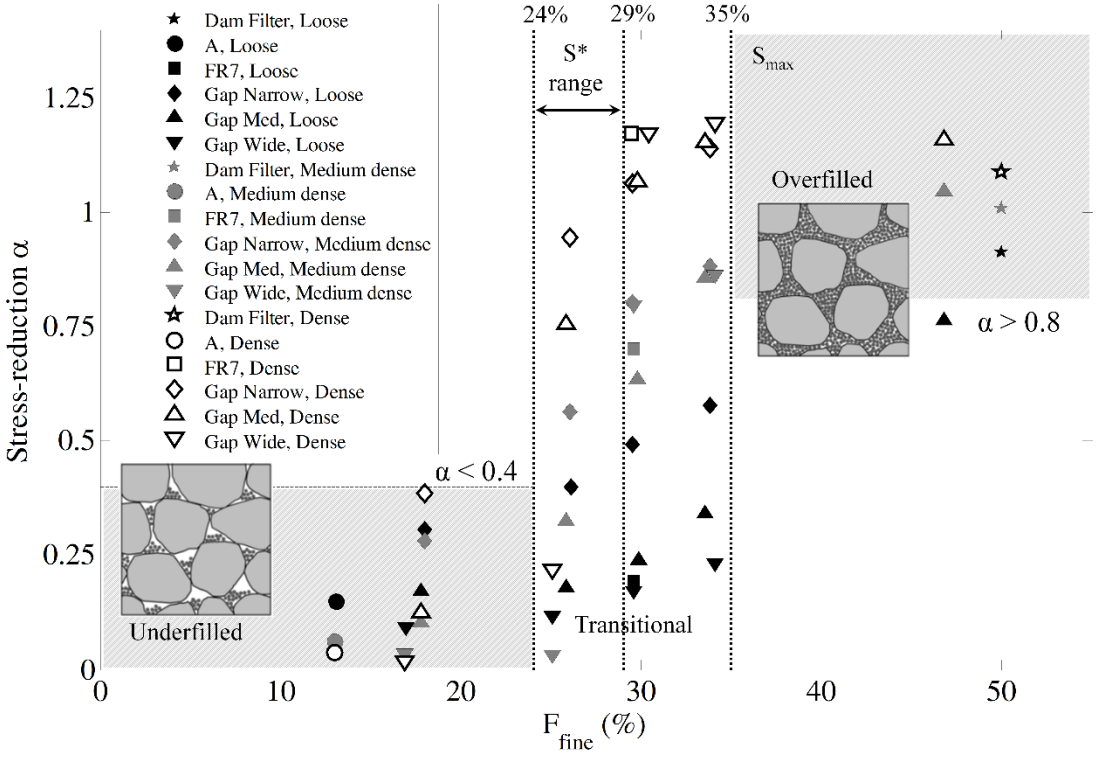

Figure 4. Variation of stress-reduction α with finer fraction.

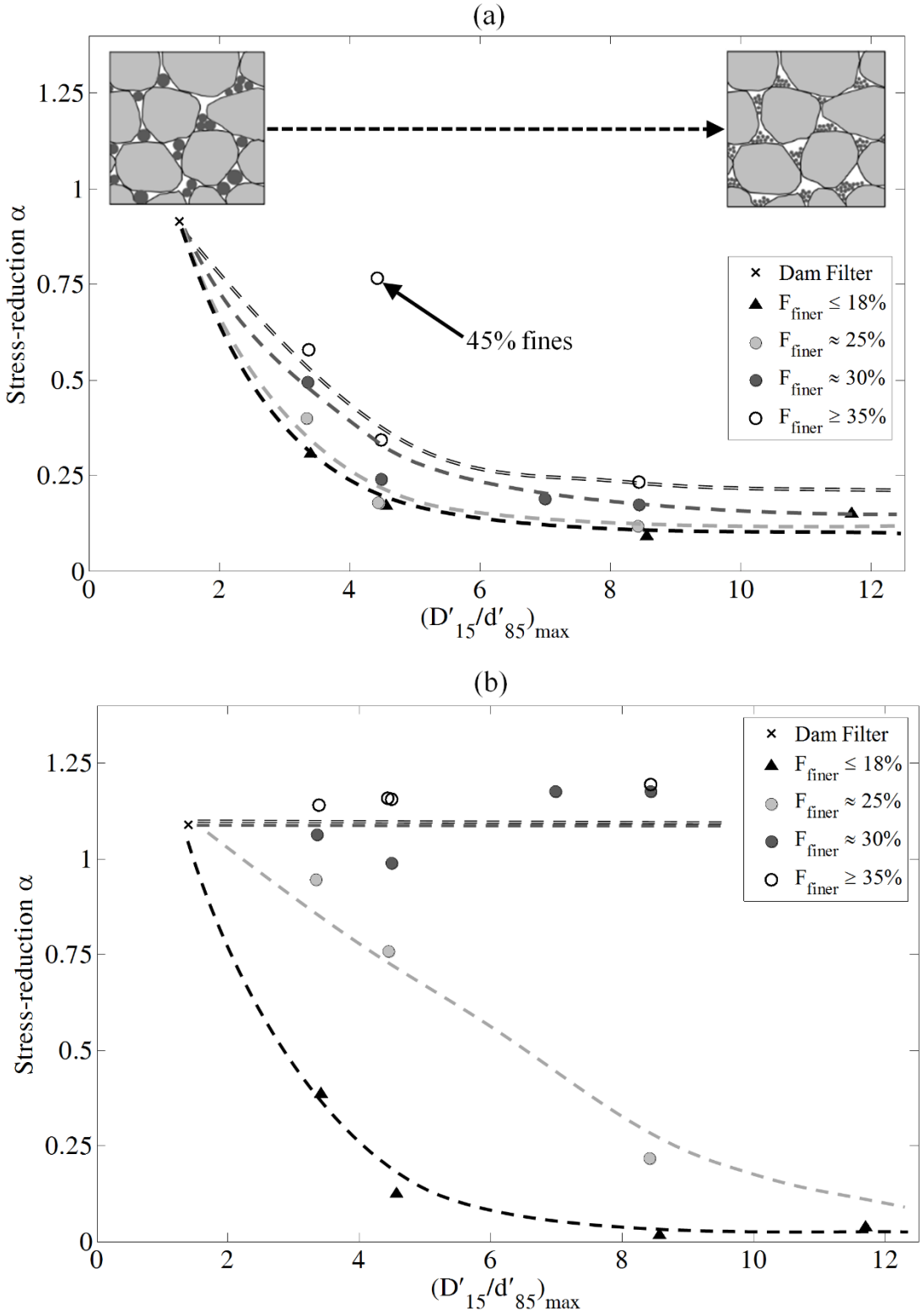

Figure 5. Variation of stress-reduction α with $(D'_{15}/d'_{85})_{max}$: (a) Loose; (b) Dense.

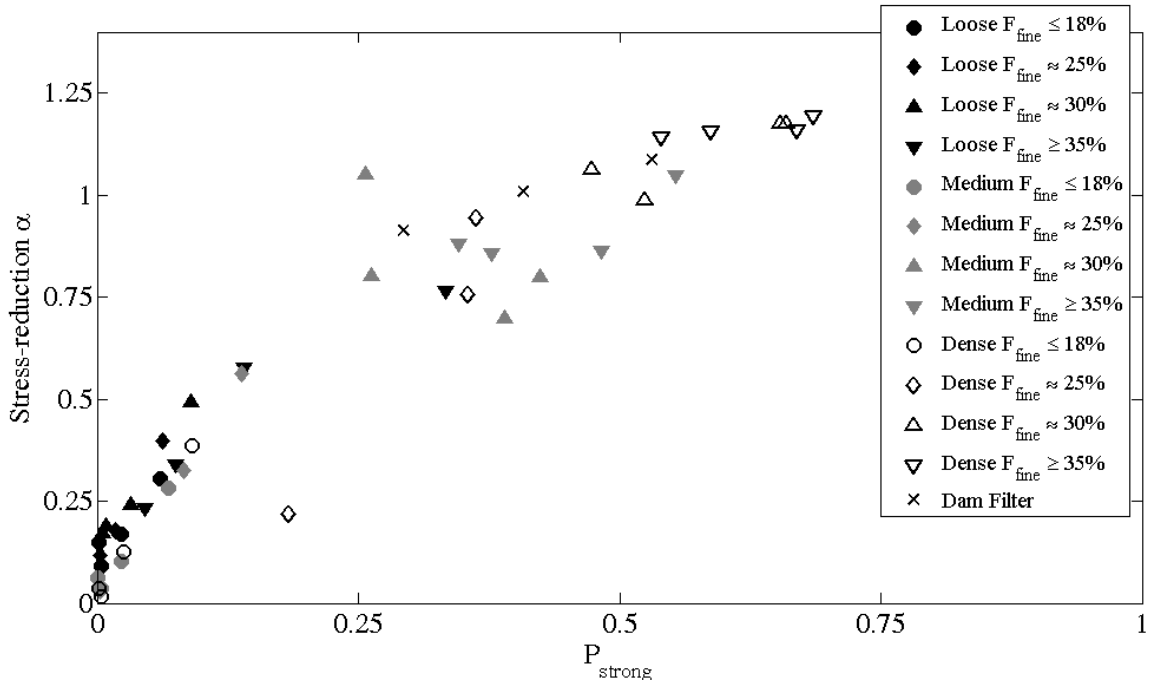

Figure 6. Variation of stress-reduction α with probability of a particle forming part of a strong force chain

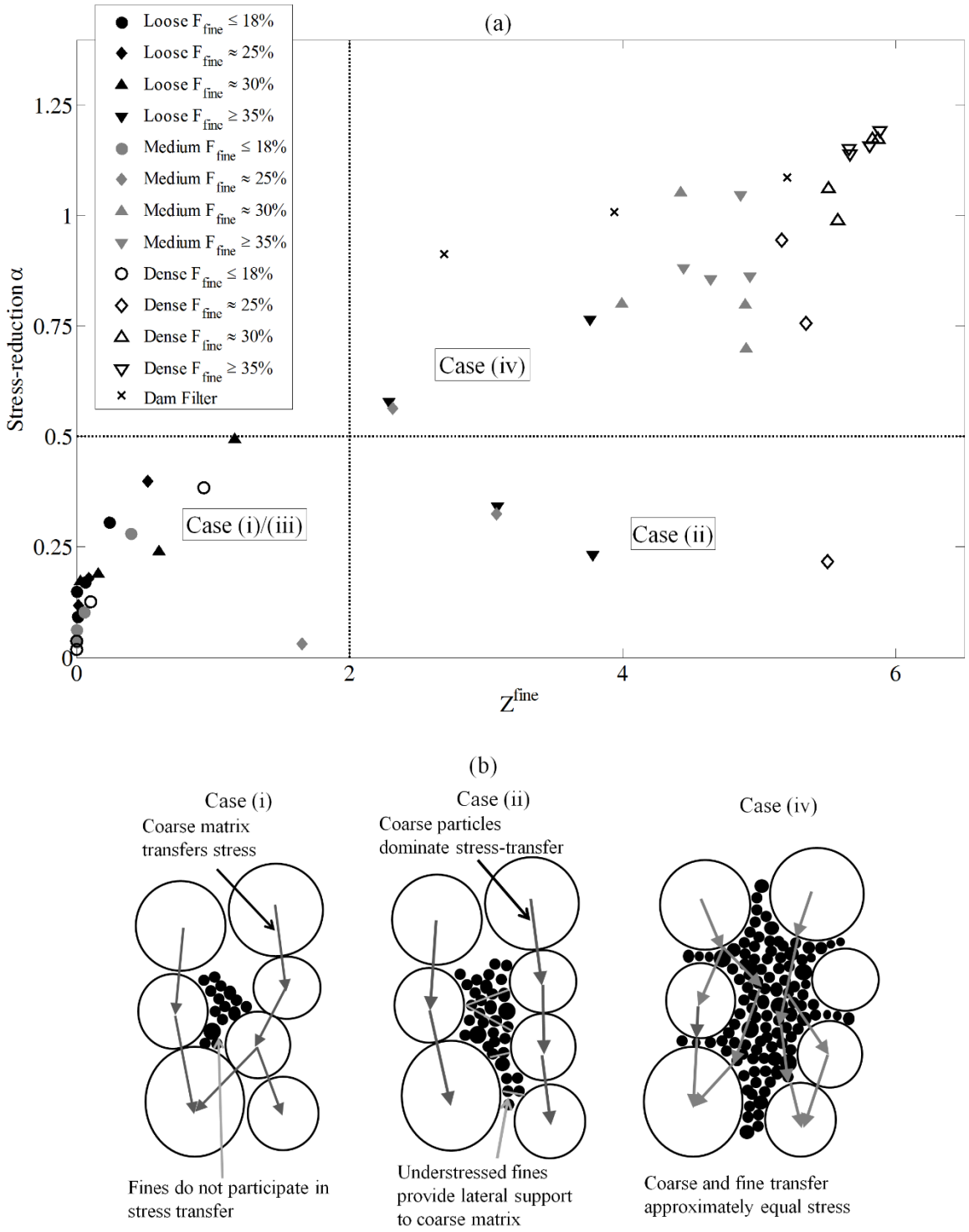

Figure 7. (a) Variation of stress-reduction α with fine-coarse coordination number; (b) Fabric cases identified by Thevanayagam et al. (2002)

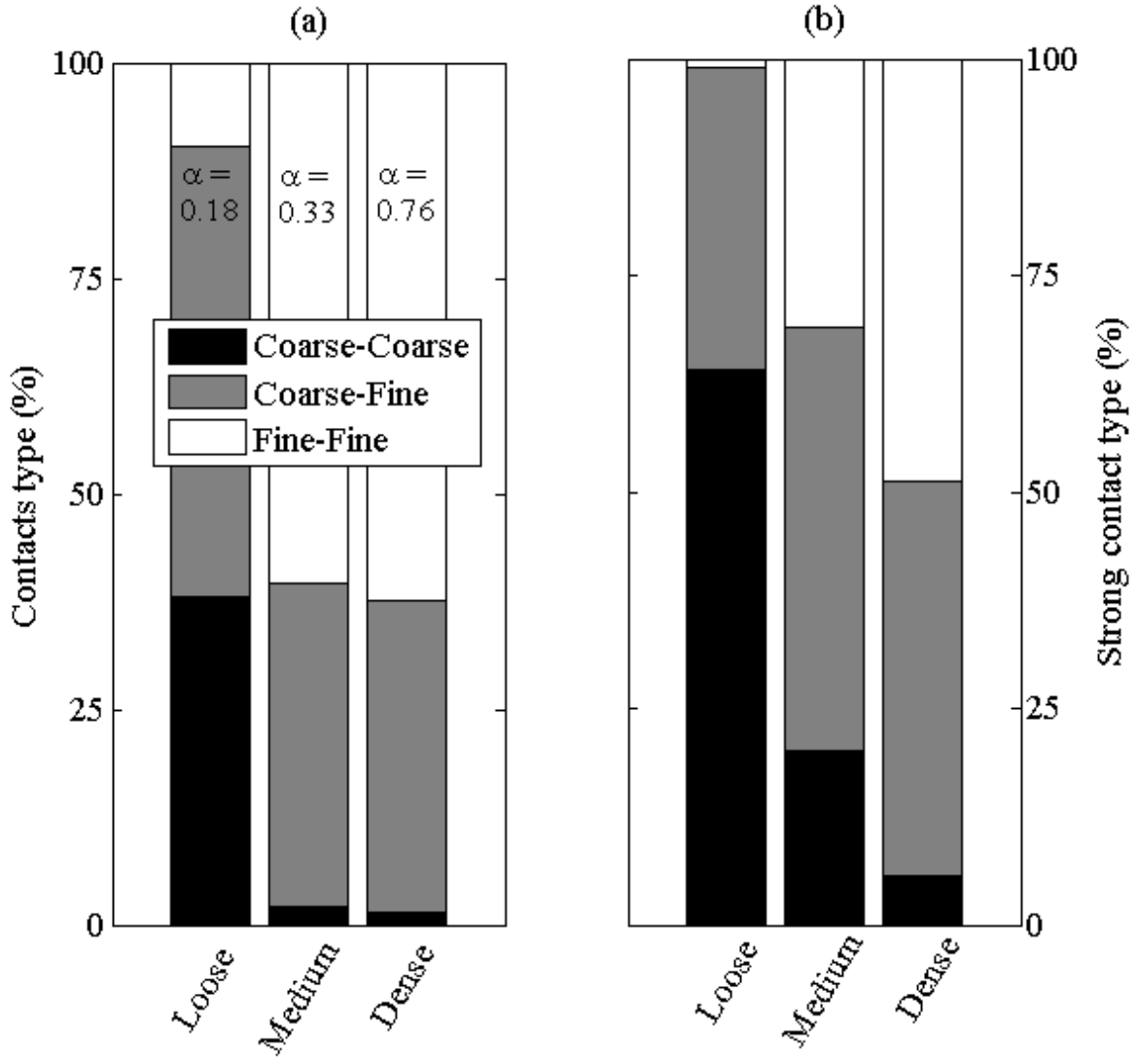

Figure 8. Contact types within sample Gap Med 25: (a) all contacts; (b) “strong” contacts only

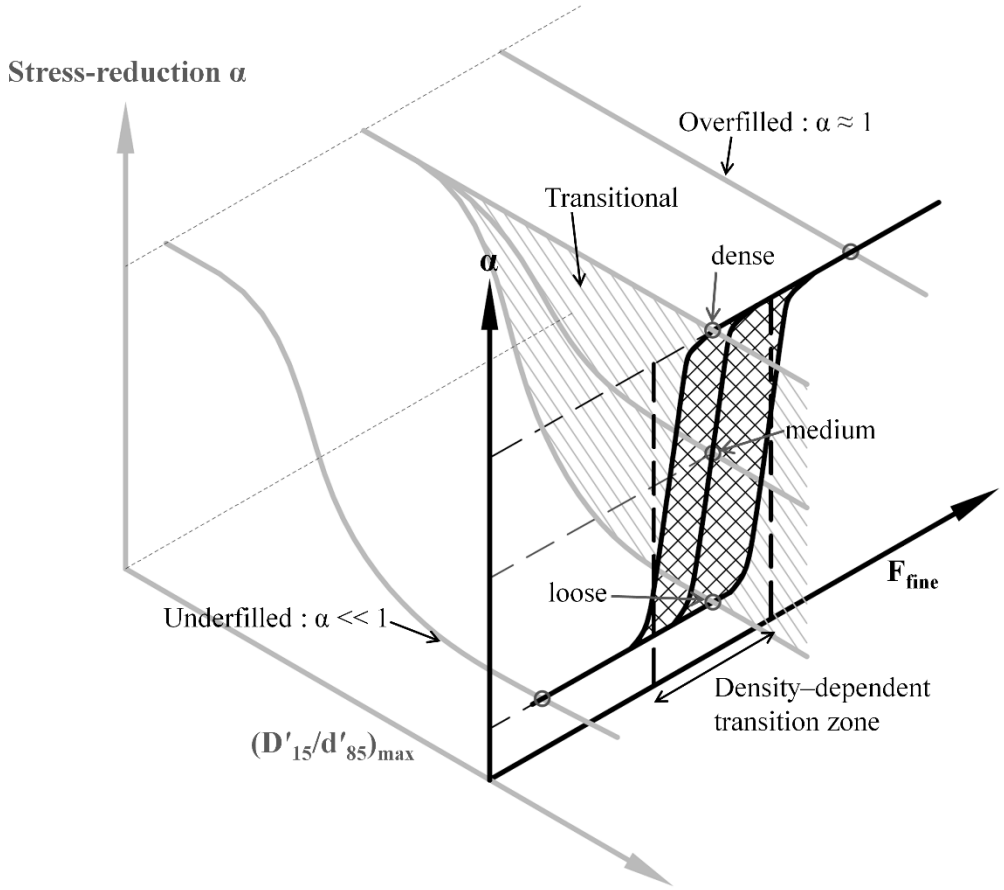

Figure 9. Factors affecting stress transfer.